2. HTRA Instrumentation I

PHILIP A. CHARLES[1]

Abstract

The range in wavelength and time resolution of current instrumentation for carrying out astrophysical studies has increased dramatically over the last five decades. Here I will give a brief historical review of time-domain astronomy, followed by a summary of the facilities available now from X-ray to near-infrared wavelengths. I will then give a glimpse of various remarkable technologies under development for the next generation of ground- and space-based observatories that will take such studies to unprecedented levels.

2.1. Introductory Remarks

First, what exactly is 'high time-resolution' for astronomers? Even today, there are those for whom the answer will be 10 minutes, while for others it is 10 microseconds! It has certainly been moving to ever shorter times over the last 50 years, and it is set very much by both the technology in use and the wavelength range in which it is applied. However, even when the field has a paucity of photons, there is a growing expectation of timing the arrival of those photons with the microsecond capability we all now effectively take for granted with the global GPS network. Achieving that is often a different matter!

This chapter is based on a series of lectures at the XXVII Canary Islands Winter School of Astrophysics on the physical instrumentation with which we undertake research in HTRA. I begin with a brief historical overview of the subject, which is almost entirely post–Second World War and driven significantly by developments in space astronomy, particularly those in high-energy astrophysics. Then I examine the range of HTRA instrumentation available today across a very broad spectrum, from both ground- and space-based facilities. Finally, I look at the latest technological advances and what they will hopefully mean for future HTRA.

This chapter is structured to provide a quick reference for the relevant literature on HTRA instrumentation and current developments. It loosely follows the lectures that I presented at the Winter School.

2.2. History of HTRA from the 1960s to the 1990s

Even by the end of the 1950s, observational astronomy was limited to optical and radio wavelengths and to timescales of a second or longer (at the very best). But this was to change dramatically in the 1960s and 1970s as space technology opened up windows to the universe all the way from γ-rays to the far-IR (FIR), regions from which we had been excluded on the ground as a result of atmospheric absorption. This is shown very nicely in figure 2 of Harwit (2003), which reviews the accessible wavelength regions and observable time resolutions as a function of decade. Indeed, what is remarkable is how these new windows all immediately had time resolutions of $\sim 0.01\,\mathrm{s}$ available, and by

[1] I am grateful to the organisers of the Winter School, Tariq Shahbaz and his Local Organising Committee, for the opportunity to deliver these lectures. I am also grateful to the Instituto de Astrofísica de Canarias and its Director, Professor Rafael Rebolo, for their hospitality at that time and subsequently during the preparation of this manuscript.

https://doi.org/10.1017/9781316831984.003 Published online by Cambridge University Press

Table 2.1. HTRA Science Drivers and Typical Timescales

Objects	Physical Process	Timescales (now)	Timescales (2020s)
AGN	Flares	mins–hours	secs
	Light-crossing time		
BH Binaries	ISCO*	ms	
	Disc flares V∼16	∼20 ms	∼1 ms
	″ ″ V∼22	5–10 s	
	Opt/X-ray correlations	<5 s	
LMXBs/CVs	Eclipse timing		
	Disc flickering	∼0.1s	≤1 ms
	Correlations/QPOs		
Pulsars	Magnetospheric	>1μs	∼ns
	Thermal	10 ms	<1 ms
	X-ray bursts	1 ms	>1μ s
Solar System	Occultations	50 ms	∼1 ms

*Innermost stable circular orbit

the turn of the millenium, this had improved to approaching 1 μs across almost the entire electromagnetic spectrum. The *time domain* for astronomical research has opened literally within a single human lifetime.

Harwit's review goes on to point out how various revolutionary astronomical phenomena are only revealed once these windows are opened with appropriate time resolution. Excellent examples include the discovery of radio pulsars, GRBs (γ-ray bursters), X-ray bursters and millisecond X-ray pulsars, and Table 2.1 is an update of that in Shearer (2008) for HTRA science drivers, the typical timescales achievable with current technology together with that under development for the next decade.

2.2.1 *Fast Optical Photometry in the 1950s and 1960s*

Even in the pre-computer era, it was possible to undertake fast (∼seconds) photometry with non-imaging, photoelectric photometers, albeit of relatively bright objects, such as cataclysmic variables (CVs). Indeed, using only a chart recorder as the output device for his photomultiplier tube (PMT), Walker (1956) was able to see coherent oscillations at a period of 71 s in the traces produced by the CV, DQ Her. This was an early glimpse of 'high-energy' processes near a compact object – as it is now recognised to be a rapidly spinning magnetic WD. Of course, using data on chart recorders was the only way of examining radio data, and that is exactly what Jocelyn Bell Burnell was doing when she discovered the first radio pulsar in 1967. The fastest of the early pulsars found was the Crab (at 33 ms), and even with the rudimentary technology of the time, its optical counterpart (a 15th magnitude star that had been seen for years on photographic images of the Crab Nebula) was found to be pulsating with the same period.

It was the arrival of the first mini-computers in the early 1970s that combined with PMTs to really open up these high-speed studies, providing a dramatic improvement on the many-minutes, limiting time resolution of photographic plates. This technology was superbly exploited by Warner and Nather with their Texas/UCT photometer in uncovering many surprising phenomena in their studies of close, interacting binaries. Indeed, it contributed significantly in building up our current picture of such systems, obtained from time-resolved eclipse studies, dwarf-nova oscillations, disc flickering, etc.

https://doi.org/10.1017/9781316831984.003 Published online by Cambridge University Press

2.2.2 *HTRA in Space*

It was during this same time period that regular access to space began, starting with rocket flights in the 1950s and 1960s. These rocket flights discovered the first cosmic X-ray source in 1961 (Sco X-1), which subsequently led to the first X-ray satellite in 1971 (*Uhuru*). However, identifying these first X-ray sources was a challenging problem as those early X-ray experiments had very poor angular resolution (typically degrees). But the nature of X-ray detectors on spacecraft meant that they had very good time resolution, so various techniques were developed that translated temporal resolution into spatial information. The simplest way was to wait until the moon was passing across regions containing X-ray sources of interest, at which point rockets were then launched in order to time the lunar occultation. The moon's position in the sky was very precisely catalogued, and so the time would tell you exactly where the X-ray source was located. The early identification of the Crab Pulsar immediately led to a rush to look for similar optical counterparts to other rapid radio pulsars, such as that in the Vela remnant, spinning only slightly slower with a period of 89 ms. However, these proved fruitless, and it took more than a decade before its 23rd magnitude counterpart was discovered. Indeed, even today, there are only five other optical pulsar counterparts known, and all, apart from the Crab, are fainter than Vela (the faintest, Geminga, is at 26th magnitude!).

2.2.3 *X-ray Detector Technology*

The first two decades of X-ray astronomy were dominated by usage of X-ray proportional counters as the detector, shown schematically in Figure 2.1. The principle is simply an extension of the Geiger counter. The operating voltage of the anode is set such that an X-ray photon entering through the thin plastic detector window ionises the gas inside, creating a cloud of photoelectrons that drift rapidly towards the anode. The causes further ionisations through internal collisions, thereby amplifying the number of electrons and producing a final pulse at the anode, the size of which is *proportional* to the energy of the incident photon. Whilst this clearly has no imaging capability, the pointing direction of the detector is controlled through a simple honeycomb collimator mounted directly above (and helping physically support) the window, restricting the field of view to be a fraction of a degree or so. Some positional information could be added to this detector by

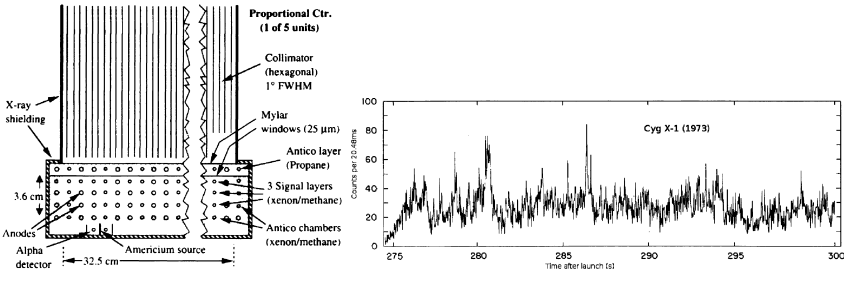

FIGURE 2.1. (Left) Schematic of one of the *RXTE* PCA's five X-ray proportional counters (Bradt et al., 1993). X-rays are collimated into the sealed counter through a thin window where they ionise the enclosed mixture of xenon and methane, producing a cloud of photoelectrons that are then attracted to the $\sim 2\,\mathrm{kV}$ anodes. Note the surrounding anti-coincidence chambers, which are blind to cosmic X-rays but are sensitive to cosmic rays and other energetic particles, thereby greatly reducing the background count rate. Reproduced with permission ©ESO. (Right) Early demonstration of the power of LAPCs, a rocket-borne observation of Cyg X-1 (Rothschild et al., 1974) displaying extremely rapid erratic variability and flickering, now considered the hallmark of BHXRBs. ©AAS. Reproduced with permission.

https://doi.org/10.1017/9781316831984.003 Published online by Cambridge University Press

making the anode resistive and timing the X-ray pulse arrival time at each end. A 2-D version of this (using a resistive disc as the anode with read-outs at the four corners) was the Imaging Proportional Counter (IPC) at the heart of the first X-ray imaging satellite (the *Einstein* X-ray Observatory).

Given the importance of proportional counter technology over the last 50 years, it is worth looking at its properties in more detail. If the detector gas has an ionisation energy of weV, then an incoming X-ray of energy, E, initially will produce $N(= E/w)$ photo-electrons, initially, which are subsequently amplified via collisions within the chamber en route to the anode (w is 26.2 eV for Ar, 21.5 eV for Xe). This process induces fluctuations that are lower than expected from Poisson statistics, with a variance $\sigma_N^2 = F.N$, where F is the Fano factor, whose value is 0.17 for Ar and Xe. The resulting energy resolution is

$$\frac{\Delta E}{E} = 2.35\frac{\sigma_N}{N} = 2.35\sqrt{\frac{wF}{E}}, \tag{2.1}$$

which is obviously poor (approaching 100 per cent) at low energies, and limited their spectroscopic capabilities in early soft X-ray surveys. Typically, $\Delta E/E = 0.4E^{-1/2}$, and the energy range of the detector is governed by (a) the window material and thickness at low E, and (b) the gas mixture and its pressure at high E. In practice, early rocket and satellite X-ray survey experiments were mostly limited to the 0.2–20 keV range.

The sensitivity of proportional counters is set by the background count rate against which X-ray sources are observed. This background is made up of two components: (i) a local (solar wind-generated) charged particle background, B_1, which will scale with detector volume; and (ii) a diffuse, uniform (across the sky) X-ray background, B_2, which is entirely astronomical in origin (at low energies, it is dominated by the $\sim 10^6$ K gas of the local interstellar medium (ISM), itself due to old supernova remnant (SNR) shocks, whereas at higher energies it is due to myriad unresolved, distant AGN). This means that the background counts detected in a t seconds observation will be $(B_1 + \Omega A B_2)t$, where Ω is the solid angle of the detector of effective area A. Consequently, the S/N ratio, σ_{SNR} obtained from a source of strength S, is

$$\sigma_{SNR} = \frac{SAt}{\sqrt{(B_1 + \Omega A B_2)t}} \tag{2.2}$$

and hence will only increase as $A^{1/2}$, a feature of non-imaging systems, and ultimately limited by source confusion to sources brighter than $\sim$ mCrab. Moving to imaging systems drastically reduces the detector volume and hence the background count rate, so sensitivity can be improved by orders of magnitude. But X-ray imaging telescopes have nothing like the collecting area of simple proportional counters, and so, for HTRA work, the latter are still by far the best technology to use. Indeed, the pulse detection in a proportional counter takes $\sim 1\,\mu$s (limited only by the ion mobility), and because the background is not varying, the S/N ratio for variability work will increase as A. The power of this simple technique is nicely demonstrated in a mere 25 s of data obtained during a rocket-borne proportional counter observation of Cyg X-1 (see Figure 2.1, from Rothschild et al., 1974), which revealed extremely rapid, erratic variability and flickering – now accepted as the hallmark of a BH X-ray binary. And from the practical point of view of limiting telemetry to data associated with real X-ray photons only, the on-board detector processing can use various techniques (guard counters and pulse-rise-time discrimination) to discard background events. Figure 2.2 shows the AstroSat Large Area X-ray Proportional Counters (LAXPCs), the most recent mission to incorporate these large-area proportional counters for HTRA X-ray astronomy work.

https://doi.org/10.1017/9781316831984.003 Published online by Cambridge University Press

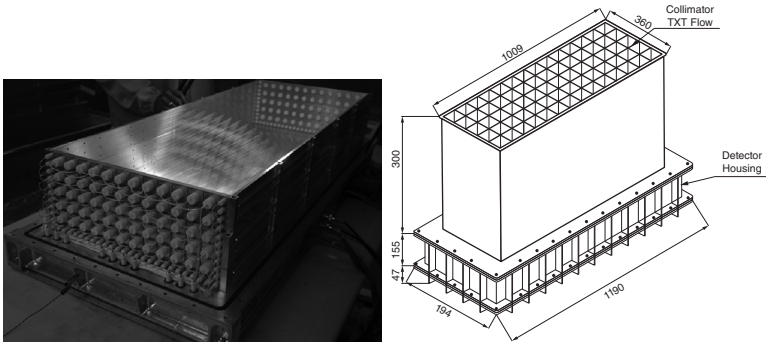

FIGURE 2.2. AstroSat LAXPC detector (left) during testing prior to its launch in 2015, and schematic (right) showing the mechanical collimator in place above the detector. (From AstroSat Handbook, courtesy of Space Science Programme Office of ISRO.)

In terms of obtaining accurate ($\sim$ arcmins) locations of the bright X-ray sources, an earlier technique that was used to convert temporal information into spatial locations was to modulate the collimator of the detector (e.g., by rotating it) around a known pointing position. This provided a modulation to a bright X-ray source's signal by an amount that depended on where it was relative to the pointing position and was the method by which Sco X-1 and others were first located and identified.

But the major step forward in X-ray astronomy came with using standard proportional counter technology on a satellite mission, and that was *Uhuru* in 1971. The greatly extended observing times combined with excellent (sub-second) time resolution immediately led to the discovery of X-ray pulsars, in particular Her X-1 and Cen X-3, with periods of a few seconds. But the extended observing time revealed that both were also eclipsing systems with obvious orbital periods of a few days. This was followed by a number of highly successful X-ray astronomy missions in the 1970s (OAO-Copernicus, OSO-8, SAS-3, ANS, Ariel-V, HEAO-1), culminating with the first true imaging mission, NASA's *Einstein* Observatory.

The first European Space Agency (ESA) mission of the 1980s combined both conventional proportional counters and X-ray imagers in their *EXOSAT* observatory, but it had one radically different approach compared to any previous astronomical satellite, and that was a spacecraft orbit that was inspired by the early lunar occultation experiments of the 1960s. ESA launched *EXOSAT* into an extremely high (two-thirds of the way to the moon) and long ($\sim$ 4 d), elliptical orbit that would enable it to eventually be able to observe lunar occultations of almost every bright X-ray source.[2] Whilst that feature was never actually exploited, it was the long satellite orbit that would make *EXOSAT* a revolutionary tool for HTRA, and that was because it allowed for long, uninterrupted observations of X-ray sources. This is in contrast to all conventional low-Earth spacecraft, whose $\sim$ 100 min orbits are punctuated by Earth blockage and restricted operations in charged-particle regions, leading to typical observing efficiencies of only $\sim$ 40 per cent, making studies of short-period X-ray binaries much more difficult. It was the success of *EXOSAT*'s orbit that led to it being adopted by both the major X-ray observatories of the current era. However, while this extended orbit does lead to a much higher overall

[2] Because of the long gestation time of *EXOSAT*, by the time it was launched in 1983, the advent of X-ray imaging telescopes meant that the occultations were superfluous, and not a single one was observed.

https://doi.org/10.1017/9781316831984.003 Published online by Cambridge University Press

observing efficiency, it does leave the spacecraft well outside Earth's magnetosphere and hence unprotected from the intense particle storms that can occur during solar flares. When these happen, the instrumentation has to be shut down.

2.3. Current Major Facilities for HTRA from X-ray to IR Wavelengths

Large-area proportional counters (LAPCs) have been in use for >50 years, and they are still in use today. That is because for studying the brightest X-ray sources at the highest time resolutions ($\sim\mu$s), you must have a very large number of photons, and that simply means you must have a large collecting area. There is still no easier and cheaper way of obtaining this than through the construction of LAPCs. Beginning with NASA's HEAO-1 in 1977 and ESA's *EXOSAT* in 1983, there has been an almost unbroken run of missions that had such detectors as their main components, and these are summarised in Table 2.2. Perhaps the most successful of them all so far has been the *Rossi* X-ray Timing Explorer (*RXTE*), which had a 15-year operational lifetime, leaving an enormous archive of high-quality data that the recently launched Indian mission, AstroSat, hopes to build upon.

As a demonstration of what such instruments can achieve, Figure 2.3 shows the extraordinary light curve of the X-ray transient, V404 Cyg, on 1989 May 30 obtained by the Ginga LAPC (Tanaka, 1989) during the peak of that outburst. Note the logarithmic scale of this plot. Even at $\sim$200,000 ct/s the detector is not saturating (it can easily handle these levels), but something within the source itself is preventing it from going above this level (possibly it is Eddington limited). And it is varying by orders of magnitude within minutes. No other source, before or since, has shown such remarkable variability. And V404 Cyg underwent a second huge, but shorter ($\sim$ 2 weeks), X-ray outburst in June 2015, but sadly this was just a few months prior to the launch of AstroSat, which in its LAXPC had what would have been the perfect instrument with which to study this outburst.

However, for studying fainter sources, LAPCs suffer from their very high particle and diffuse X-ray background, making it much harder to follow their short-term variations. It becomes essential to move to imaging systems, which allow the detectors to be much smaller in volume, and the focussing of the source X-rays enhances them with respect to the diffuse X-ray background, thereby providing enormous gains in sensitivity. To achieve

Table 2.2. Large-Area X-ray Proportional Counter Missions

Mission	Dates	Total Area (N*) (cm^2)	E range (keV)
Uhuru	70–73	840 (2)	2–20
Ariel-V	74–80	580 (2)	1.5–20
HEAO-1 A-1	77–79	10,500 (7)	0.25–25
HEAO-1 A-2 LED	″	800 (2)	0.15–3
HEAO-1 A-2 MED	″	800 (1)	1.5–20
HEAO-1 A-2 HED	″	2,400 (3)	2.5–60
EXOSAT ME	83–86	1600 (8)	1–50
Ginga LAC	87–91	4,000 (8)	1.5–37
RXTE PCA	95–12	6,500 (5)	2–60
RXTE HEXTE	″	1,600 (2)	15–250
AstroSat LAXPC	15–	10,800 (3)	3–80

*N = no. of individual PCs

https://doi.org/10.1017/9781316831984.003 Published online by Cambridge University Press

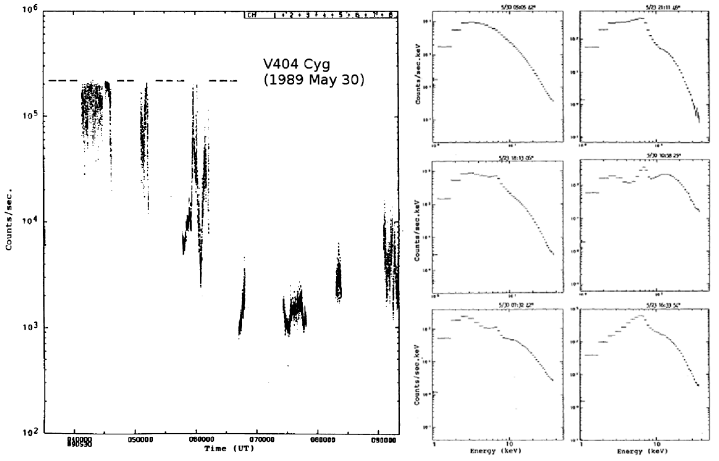

FIGURE 2.3. The LAPC on Ginga observed this extraordinary light curve (left) from the BHXRB V404 Cyg during its 1989 outburst, with associated dramatic spectral variability (right). This included large (local) changes in the X-ray absorbing column (up to $\sim 5{\times}10^{23}$ cm^{-2}). From Tanaka (1989). Credit ESA Special Publication.

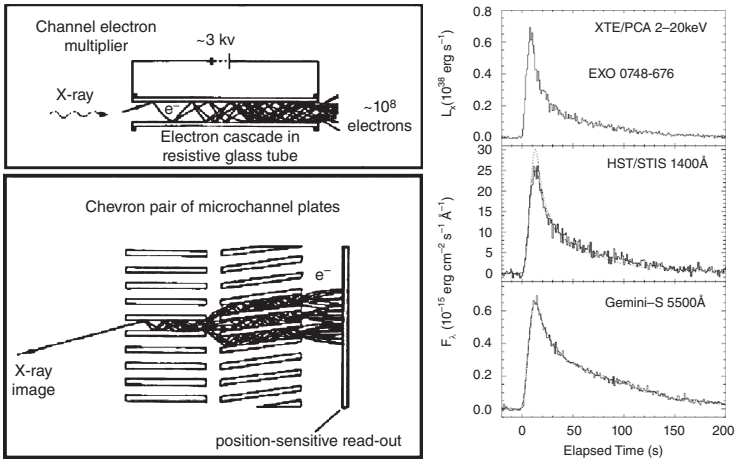

FIGURE 2.4. (Left) Microchannel plates are formed from thousands of tiny glass channel electron multipliers, each of which provides a very high gain of electron clouds produced by incoming X-rays. Normally operated as an angled ('chevron') pair so that radiation cannot pass straight through (Seward and Charles, 2010). (Right) X-ray burst from EXO 0748-676 observed simultaneously at X-ray (*RXTE*), UV (HST) and optical (Gemini-S) wavelengths, demonstrating an optical lag of 4 s with respect to the X-rays as they illuminate this LMXB's accretion disc (Hynes et al., 2006). ©AAS. Reproduced with permission.

the imaging, however, requires the use of grazing incidence X-ray mirrors, the first of which were *Einstein* and then *EXOSAT*. But this gain in sensitivity comes at a cost of collecting far fewer X-ray source photons and increased difficulty in achieving so very short time variability. And while position sensitivity is possible with proportional counters, as employed on both *Einstein* and ROSAT, there are other technologies that can achieve better spatial resolution. An example of such technology, microchannel plates (MCPs), as shown schematically in Figure 2.4, amplify the photoelectrons created by the

https://doi.org/10.1017/9781316831984.003 Published online by Cambridge University Press

incoming high-energy photon as a result of the high voltage across the plate. The resulting charge cloud is then read out and centroided in order to provide the location of the initial photon. This technique works from X-rays all the way to UV photons and formed the basis of one of the first-generation detectors, MAMA (the multi-anode microchannel array), on Hubble Space Telescope (HST), and then as both near- and far-UV detectors on *GALEX*. Unfortunately, one of the main limitations of such detectors is their maximum total count rate of $\sim$30,000 ct/s, and that is from the *entire* detector, not just from one source (and hence explains why observations even now with the *XMM-Newton* OM are restricted according to the brightest star within the target field of view).

Furthermore, the photocathode used to turn the incoming UV photons into photo-electrons has a maximum efficiency of $\sim$10 per cent, whereas modern charge-coupled devices (CCDs) are now approaching 100 per cent efficiency, so why should we continue using MCPs? The answer is that the MCPs provide photon-counting detection, which has zero noise associated with it, whereas the read-out of a CCD image has an unavoidable noise. And in the UV part of the spectrum, the sky is remarkably dark compared to the optical, and so it is possible for the lower-efficiency MCPs to provide better UV images than would be possible using CCD detectors (see, e.g., Morrissey and KCWI Team, 2011). However, there are now 'low light level' (or L3) CCDs becoming available that use on-chip amplification prior to read-out to reduce this effect (these are also known as EMCCDs, electron multiplication charge-coupled devices, see Chapter 3 by V. Dhillon in this volume for full details).

A very nice example of the use of these technologies for multi-wavelength HTRA is in Figure 2.4, where *RXTE*, HST and Gemini-S obtained simultaneous observations of the LMXB X0748-676 (Hynes et al., 2006) during which an X-ray burst occurred and was detected at all wavelengths. Furthermore, the fast timing allowed the delay of the UV and then (later still) the optical bursts with respect to the X-rays to be clearly measured. HST was using the Space Telescope Imaging Spectrograph (STIS) MAMA detector for this work, whereas Gemini-S was using its Acquisition Camera, a conventional CCD but one where binning and windowing allowed for the 1 s exposures to be read out with only $\sim$0.3 s dead time between exposures. It is also important to note that these HST data do not have absolute timing information of the same accuracy as provided by *RXTE* and Gemini-S.

2.3.1 *Solid-State X-ray Detectors*

To improve at low energies on the poor spectral resolution of proportional counters (PCs), it is necessary to move to materials that have much lower work functions in the detection of X-ray photons, and that means moving to solid-state technologies. As shown in Table 2.3 the effective energy resolution of materials such as Si (used by the first such detector, the solid-state spectrometer, or SSS, on the *Einstein* Observatory) is both far better than PCs and constant with energy. A schematic of the SSS is shown in Figure 2.5

Table 2.3. X-ray Energy Resolution

Material	w (eV)	Fano Factor	R ($=E/\Delta E$) (@ 6 keV)
Ar	26.2	0.17	5–10
Xe	21.5	0.17	″
Si	3.6	0.12	25–50
Ge	3.0	0.13	55
CdTe	4.4	0.11	3–50

https://doi.org/10.1017/9781316831984.003 Published online by Cambridge University Press

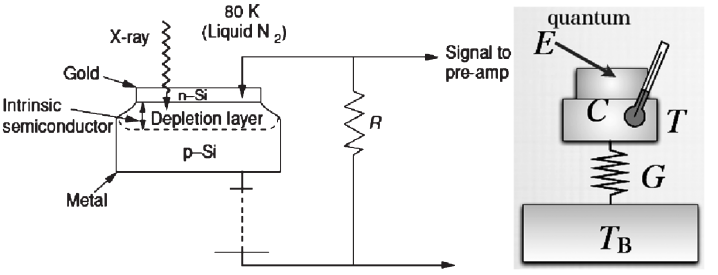

FIGURE 2.5. (Left) Schematic of the *Einstein* SSS in which incoming X-rays produce ion pairs in the Si-doped reverse-biased junction, which is maintained at 80 K so as to reduce thermal noise (Seward and Charles, 2010). (Right) Schematic of a microcalorimeter operation, as used on *Hitomi*. Incoming X-ray photons deposit energy in a very cold absorber (at 50 mK), producing a thermal pulse that is then measured (Mitsuda et al., 2010). © 2010 Society of Photo Optical Instrumentation Engineers.

(left), where a reverse-biased junction creates a depletion layer that acts as the X-ray detecting volume. Incoming X-ray photons create ion pairs, but there is no avalanche as in PCs. Consequently, to reduce noise, the detector must be cooled to 80 K and employ low-noise pre-amps. It is small in volume and is located in the focal plane of the X-ray telescope. The *Einstein* SSS was a great success but only operated for about nine months, at which point it had run out of cryogen.

Over the last 20 years, an extension of this technology to even better spectral resolution has been achieved through the development of *micro-calorimeters*, shown in Figure 2.5 (right). By maintaining the detector at ultra-low temperatures ($\leq$ 100 mK) the total energy of the incoming X-ray photon can be measured through the thermal pulse it induces, leading to an energy resolution, ΔE, which depends on the detector's temperature and thermal capacity. The device flown recently on Astro-H (launched February 2017) used an array of 32 absorbers operated at 50 mK, each of which was less than 1 mm square and only 8 μ thick, giving an energy resolution of 7 eV over the range 0.3–12 keV (Mitsuda et al., 2010). This provided the highest spectral resolution ever obtained for cosmic X-ray spectroscopy and was also combined with high time-resolution capability. Sadly, Astro-H (or *Hitomi*, as it was renamed in orbit) only worked for barely a month before an attitude control failure led to the loss of the spacecraft. Nevertheless, the power of this technology was clearly demonstrated (see the 2016 July 6 edition of *Nature*) as it provides high detection efficiency, high spectral resolution and fast timing capacity, essentially the ideal X-ray astronomy detector.

Since the turn of the millenium, the dominant X-ray astronomy missions have been *Chandra* and *XMM-Newton*, with the largest collecting areas (of grazing incidence mirrors) yet assembled. *XMM-Newton* is the largest, and *Chandra* has the finest angular resolution ($\sim$ 1 arcsec, comparable to ground-based imaging, neither of which are likely to be superseded for at least a decade. Both use arrays of CCDs as their X-ray detectors, but they are used in photon-counting mode rather than as integrating devices as in the optical. That is because the X-ray photon flux is much smaller than in the optical (and the telescopes' effective areas do not compare with conventional telescopes) and each X-ray photon deposits far more energy in the CCD, thereby producing many more photelectrons. Indeed, as for the SSS, the energy resolution of CCDs is far higher than PCs, and so the full range of attributes (location, time, energy) can be measured for each individual photon. It is these data that are transmitted to ground, rather than full images, as the data rate is then far lower. The CCDs employed are 1024 $\times$ 1024 devices.

https://doi.org/10.1017/9781316831984.003 Published online by Cambridge University Press

TABLE 2.4. X-ray CCD Missions

Mission	Dates	E Range (keV)	Effective Area (cm^2@1 keV)	ΔE (@6 keV)
ASCA	93–01	0.4–10	1300	2 %
Chandra	99–	0.2–10	340	1–5 %
XMM-Newton	99–	0.1–15	∼1000	2–5 %
SWIFT – XRT	04–	0.2–10	125	2 %
Suzaku – XIS	05–15	0.2–12	∼1000	2 %
AstroSat – SXT	15–	0.3–8	125	2.5 %

TABLE 2.5. *XMM-Newton* EPIC Timing Capabilities for Point Sources

MOS Central CCD (pixels)*		Time Resolution (millisecs.)	Live Time (%)	Max. Count Rate (s^{-1})	[mCrab]
600×600	Full frame	2600	100	0.50	[0.17]
300×300	Large window	900	99.5	1.5	[0.49]
100×100	Small window	300	97.5	4.5	[1.53]
100×600	Timing (1-D)	1.75	100	100	[35]
pn CCDs					
(pixels)†					
376×384	Full frame	73.4	99.9	2	[0.23]
198×384	Large window	47.7	94.9	3	[0.35]
63×64	Small window	5.7	71.0	25	[3.25]
64×200	Timing (1-D)	0.03	99.5	800	[85]
64×180	Burst (1-D)	0.007	3.0	60,000	[6,300]

*1 pixel = 1.1 arcsec
†1 pixel = 4.1 arcsec

This means that with 1 s binning and 16-bit encoding, full images would require a 16 Mb/s data stream, which is not manageable. Instead, event lists of $[x, y, t, E]$ are compiled on-board, and this makes a much lower data rate to be transmitted for subsequent processing on the ground. Thus, this allows observers to subsequently generate X-ray images in whatever time or energy bin they require for the nature of the observation, a very powerful feature. This technology was first used in the Japanese *ASCA* mission, equipped with ∼5 times the *Einstein* collecting area, but with CCDs providing far better spectral resolution than the IPC. Such detectors are also part of the *ASCA*, *SWIFT* and *Suzaku* missions (see the summary in Table 2.4).

But these devices have significant limitations for high time-resolution work: the read-out demands of CCDs provide serious constraints on their use for HTRA, as the on-board processing of individual photons to determine their 2-D position limits the time resolution to a few seconds. However, there are approaches available to improve the time resolution to the order of milliseconds, by using a *windowed* timing mode, in which the image is reduced to 1-D only, but the full spectroscopic capability is still available. Of course, this only works for bright sources, as there will be an increased background level. This range of options is nicely demonstrated in Table 2.5, which lists the fast timing options that are available from *XMM-Newton*'s European photon imaging camera (EPIC)-pn cameras. In normal operation, time resolution is limited to ∼0.2 s, but this can be extended down to ∼5 ms with the windowing technique. However, all of these

https://doi.org/10.1017/9781316831984.003 Published online by Cambridge University Press

are restricted to relatively faint sources of a few mCrab (up to 25 mCrab with the small window), otherwise pile-up (multiple photons arriving during the CCD observing interval) will occur. There are special non-imaging timing modes that can reach 30 μs (for sources of < 800 mCrab), or even 7 μs for the very brightest sources (up to 60 Crab), but the efficiency of operation of this latter option is extremely low (3 per cent). This is thus a very different operational region from that available to LAPCs. Similar restrictions apply with *Chandra*. However, both *XMM-Newton* and *Chandra* are in high, ~ 4 d, orbits that permit extended, uninterrupted viewing of sources for many hours at a time, sometimes even days. This is a particularly valuable tool to use on short-period ($\sim$ hours) X-ray binaries that show variability on orbital and super-orbital timescales (e.g., Smale et al., 1988).

The *SWIFT* X-ray telescope provides an observing capability that complements all those described so far. Its name is not an acronym but an indication of its principle operational mode, namely the ability to respond *swiftly* to transient events, thereby providing a 'high time-resolution' mode of a completely different nature than what had been available hitherto. Targeted of course at GRBs, it can slew and begin observing with its X-ray telescope and optical monitor (OM) within minutes of the detection and approximate localisation of a GRB, a feature that has been critical to its huge success in this field (and very dramatically better than the $\sim$days response possible with earlier high-energy missions). However, such a capability is also perfect for studying new X-ray transients or following state changes in a wide range of X-ray binaries and monitoring (via many short observations) over transient outbursts or through periods of unusual source behaviour, and *SWIFT* has been extremely productive in these ways over its lifetime, as recently reviewed by Gehrels and Cannizzo (2015), Kennea (2015) and Levan (2015).

Extending X-ray imaging capability to high-energy X-rays (significantly above 10 keV) has been recently achieved through the NuSTAR mission (Harrison, 2015). Since 2000, developments in multi-layer coating of grazing incidence optics have given NuSTAR an operational energy range of 3–79 keV, combined with an angular resolution of about an arcminute. Given the lower photon fluxes and much higher particle background at these energies, such an imaging capability has drastically improved sensitivity compared to earlier missions.

2.3.2 *Optical/IR Detector Developments*

CCDs are very much the workhorse detectors for a wide swathe of astronomical studies. But their (relatively) extended read-out times and associated read-out noise provide limitations that require workarounds for HTRA, as discussed above for X-ray applications. Similar issues apply at ground-based observatories, and windowed read-out (to reduce read-out times from minutes down to a few seconds) has been used since the early days of CCDs. A significant improvement came about 20 years ago through frame-transfer devices, whereby the CCD can be divided into two electronic halves, one to act as the live imager, which shifts the image at the end of each exposure very rapidly ($\sim\mu$s) into the read-out half. The image can then be read out while the 'live' half continues in parallel with the next exposure (thereby eliminating the dead time associated with each read-out). Two extremely successful instruments, the UCT/CCD (O'Donoghue, 1995) and ULTRACAM (Dhillon et al., 2007) have operated in this way since the mid-1990s onwards, and full details of this and the latest CCD developments are dealt with in Chapter 3 by V. Dhillon in this volume.

Since 2000, there have been developments in optical photon-counting detectors, and we will now look at two of these developments.

https://doi.org/10.1017/9781316831984.003 Published online by Cambridge University Press

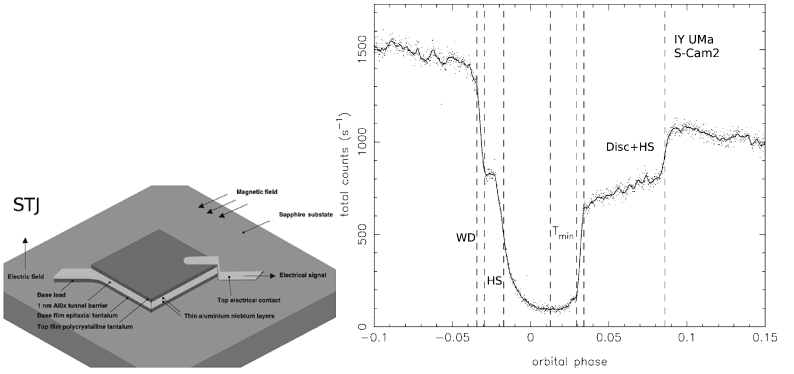

FIGURE 2.6. (Left) Schematic of one tantalum element (which is 25 μ square) of an STJ device, as used in S-Cam2, and which is operated at 0.32 K. Incoming photons deposit energy in this element, thereby breaking Cooper pairs in the superconductor and releasing free electrons in proportion to the energy of the incident photon. Credit ESA. (Right) S-Cam2 light curve of the eclipsing dwarf nova IY UMa, obtained with the William Herschel Telescope (WHT). Times of eclipse of the WD and hot spot (HS) are marked, as are the emergence from eclipse of the disc and HS (Steeghs et al., 2003).

1. *STJs*

   Developed at ESTEC, S-Cam is based on the superconducting tunnel-junction (STJ) detectors used from the mm to far-IR bands both on the ground and in space. As part of a research program to exploit this technology at X-ray energies, it was recognised by Perryman et al. (1993) and demonstrated by Peacock et al. (1996) that it could be extended to work at optical wavelengths as well (indeed, providing the first non-filtered measurement of the energy of an optical photon). Shown schematically in Figure 2.6, the incident photons break Cooper pairs in the superconductor. Furthermore, the detected optical photon would produce a sufficient number of electrons in this process to provide some (R$\sim$ 10–50) spectral information as well. Given that they work well over the entire visible spectrum with close to 100 per cent quantum efficiency (QE), provides $\sim$1 μs timing accuracy and non-dispersive, albeit crude, spectroscopy, they have the potential to become the 'ideal' astronomical detector. Their main limitation is the practical difficulties associated with (a) producing arrays of these devices (current versions have been small, typically <40 pixels), and (b) maintaining them at their operating temperature of <1 K!

   Nevertheless, an implementation of this technology (S-Cam2) has been used to observe the Crab Pulsar and an eclipsing binary, UZ For (Perryman et al., 2001). The CVs IY UMa and HT Cas (see Figure 2.6) were observed by Steeghs et al. (2003) with this camera, and the intrinsic R$\sim$10 is sufficient to be able to separate the large amplitude blue spectral flickering from the WD and cooler regions.

2. *Intensified CCDs*

   It is possible to use CCDs as part of much higher time resolution instruments if additional pre-amplification of the image is undertaken. An example of such a device is the MCP-intensified CCD (or MIC) detector developed by Fordham et al. (2000), which uses a three-stage MCP front end to intensify the image produced by the photocathode before reading it out with a CCD (as shown schematically in Figure 2.7). The amplification factor is so great ($\sim 10^7$) that each photon can be individually read by a fast-read-out CCD, thereby eliminating read-out noise. While being easily applicable as detector for either imaging or spectroscopic instruments,

https://doi.org/10.1017/9781316831984.003 Published online by Cambridge University Press

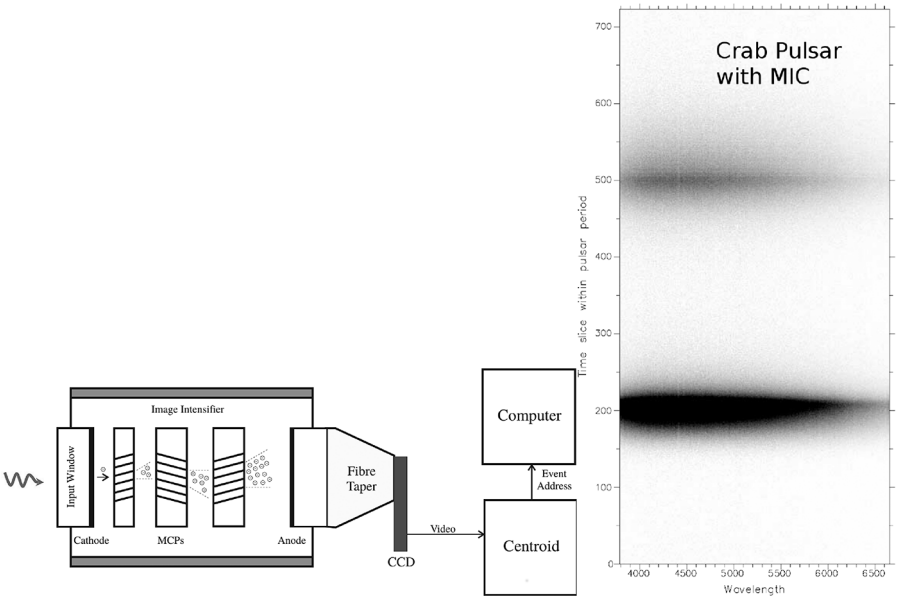

FIGURE 2.7. (Left) Schematic operation of an MCP-intensified CCD detector. Incoming photons release photoelectrons from the photocathode, which are then substantially ($\sim 5\times10^5$) amplified by the triple MCPs, prior to read-out by the CCD. The amplification increases the extent of the incoming electron cloud, and so the resulting pulse is centroided in order to produce an estimate of the incident photon location and then recorded (Fordham et al., 2000). (Right) MIC phase-resolved optical spectra of the 33.5 ms Crab Pulsar with 46 μs binning (Fordham et al., 2002). ©AAS. Reproduced with permission.

it is the (relatively poor) QE of the MCP's photocathode (typical S20 response has $\leq$20 per cent efficiency) that is the ultimate limiting factor here. Nevertheless, this device has been involved in successful campaigns at Kitt Peak and San Pedro Mártir, where the photon-counting allows the data to be binned in post-processing in ways that optimise the various science goals (see, e.g., Fordham et al., 2002, as shown in Figure 2.7).

A variant of this technology uses delay-line anodes in place of the CCD to read out the electron chargecloud location (e.g., Siegmund et al., 2008), and such devices have been used successfully in ground and space-based telescopes, from SALT (McPhate et al., 2012) to GALEX (Morrissey, 2006).

2.3.3 *2-D Time-Series or Single-Aperture Photometry?*

Clearly the approaches described above are constantly trading off the desire for a time series of the full images that CCDs and related detectors are capable of producing with the need for ever-greater time resolution that is possible if single apertures are used. The imaging approach requires the use of fixed time bins, whereas single apertures allow the time-tagging of individual photons, both producing data streams for subsequent processing. An example of the former is 'LuckyCam' (Mackay, 2013) which uses one of the new generation EMCCDs with a fast controller to take 2 ms images. At such a rate, data storage demands would be enormous, but LuckyCam only records the $\sim$10 per cent images containing the sharpest stellar images (based on a reference field star), as demonstrated in Figure 2.8. As the system is operating faster than the atmospheric

https://doi.org/10.1017/9781316831984.003 Published online by Cambridge University Press

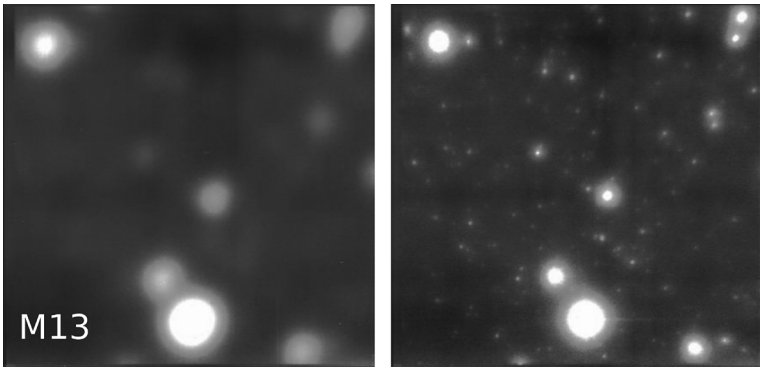

FIGURE 2.8. Images of the globular cluster M13 obtained with the Palomar 5 m telescope: the left image shows the natural seeing of ∼0.65 arcsecs, whereas the right used the 'lucky imaging' technique to achieve ∼35 milliarcsecs resolution. At the time, this was the highest resolution optical/near-infrared image *ever* obtained (and about three times better than HST!) (Mackay et al., 2012). © 2012 Society of Photo Optical Instrumentation Engineers.

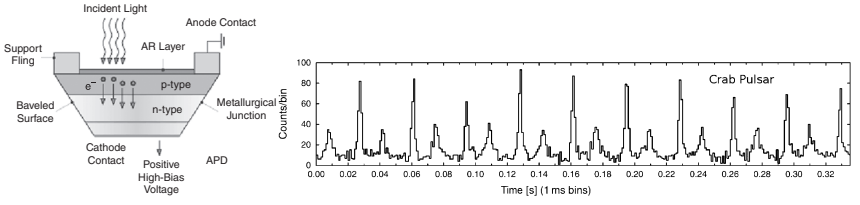

FIGURE 2.9. (Left) Schematic of an APD where the large reverse bias (∼2 kV) produces an avalanche amplification of the photoelectrons. © 2017 Society of Photo Optical Instrumentation Engineers. (Right) Individual rotations of the Crab Pulsar as observed by OPTIMA with the Calar Alto 3.5 m in January 2002 in white light and at 1 ms time resolution. From Kanbach et al. (2008).

seeing timescales (hence requiring fast CCD controllers), this allows LuckyCam to exploit the periods of the very best seeing. Such devices are now being proposed for a wide range of astrophysical problems (see, e.g., MacKay et al., 2016).

The alternative approach of single aperture, photon-counting photometry is well demonstrated by the OPTIMA (Optical Pulsar TIMing Analyzer) instrument Kanbach et al. (2008), which exploits the extremely high time-resolution capability of APDs (avalanche photodiodes see Renker, 2006). These are very simple devices that have been described as akin to Geiger counters, in that the incoming photon is detected at the ∼2 kV reverse biased pn-junction, producing photoelectrons that immediately trigger a rapid avalanche, the detection pulse, as shown in Figure 2.9. By placing seven fibre-fed apertures over the Crab Pulsar, OPTIMA has already achieved sub-millisecond time resolution to produce the light curve also shown in that figure, which reveals the detailed structure of individual 33 ms pulses.

Early in the development of OPTIMA, there was a bright X-ray transient in outburst, XTE J1118+480, which was observed simultaneously by XTE and OPTIMA (Kanbach et al., 2001) to produce the highly unexpected result of an optical dip that *preceded* (by ∼30 ms) X-ray flaring and so could not have been X-ray reprocessing (see Figure 2.10). It is almost certainly related to the jet emission processes that must have been taking place. (See Chapter 4 by T. Belloni in this volume.)

https://doi.org/10.1017/9781316831984.003 Published online by Cambridge University Press

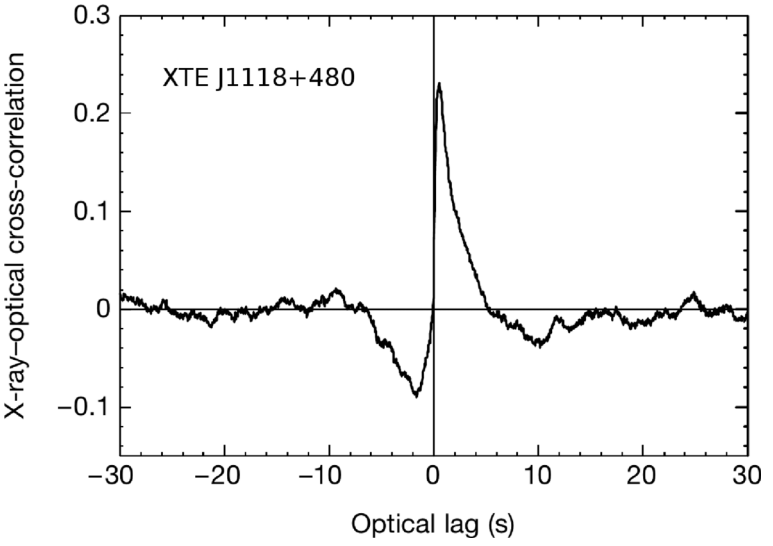

FIGURE 2.10. X-ray/optical correlation of simultaneous observations of the BH X-ray transient XTE J1118+480, by *RXTE* and OPTIMA, which shows the optical dipping a few seconds *before* the X-rays, exactly the opposite of what is normally seen (Kanbach et al., 2001).

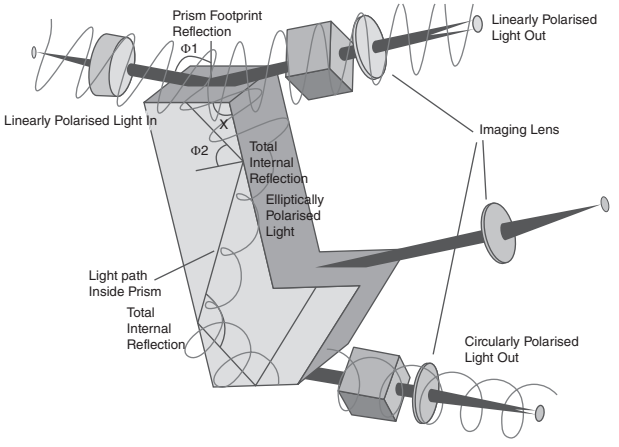

FIGURE 2.11. Optical layout of GASP, the Galway Astronomical Stokes Polarimeter. The incoming beam is split three ways, two for subsequent polarisation analysis, the other for acquisition imaging and guiding. APDs are used for detection, while EMCCDs are used for the imaging beam. (Collins et al., 2009).

The Crab Pulsar's powerful magnetic field also means that the pulsed light should be highly polarised, the details of which can provide important physical constraints, particularly during the extreme 'giant radio pulses' (Shearer et al., 2003) that are seen from the Crab and have structure on timescales of nanoseconds. Indeed, only the Crab is bright enough for ultra-high-speed polarimetry, and GASP, the Galway Astronomical Stokes Polarimeter, has been designed specifically with this object in mind, although there are limitations to what polarisation measurements are possible on such timescales, as discussed by Redfern and Collins (2008). In GASP (see Figure 2.11), the incoming

https://doi.org/10.1017/9781316831984.003 Published online by Cambridge University Press

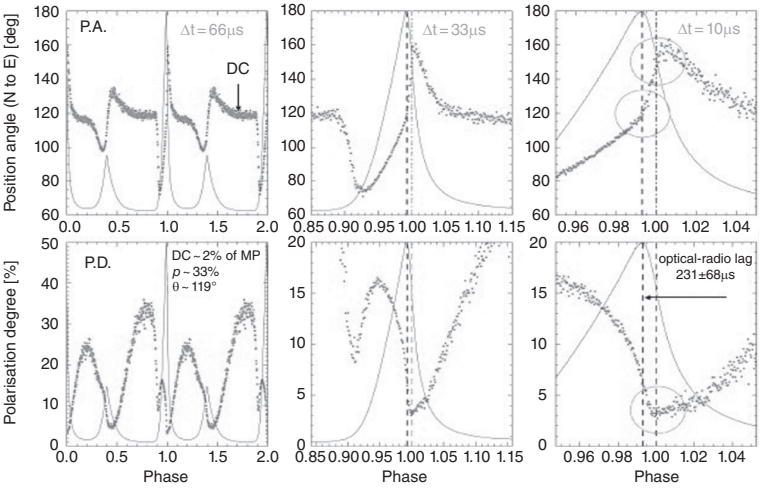

FIGURE 2.12. Observations of the Crab Pulsar using OPTIMA on the NOT, showing the $\sim 200\,\mu$s offset between the optical and radio pulses (Słowikowska et al., 2009).

light beam is divided through the modified Fresnel rhomb and subsequent Wollaston prisms into four output beams, the intensities of which are linearly related to the Stokes parameters (Collins et al., 2013). There is also an extractor beam that has a large field of view and can be re-imaged onto an EMCCD for fast guiding/photometry. The main detectors for GASP have included MCP devices with delay-line read-out anodes (Siegmund et al., 2008) and APDs. For details on the results, see Shearer (2008) and Sheehan et al. (2010).

Similarly, Słowikowska et al. (2009) used OPTIMA on the Nordic Optical Telescope (NOT) on La Palma to study the polarisation properties of the Crab Pulsar (see Figure 2.12) with a time resolution of $\sim 10\,\mu$s. These data also revealed an offset between the optical and radio pulses of $\sim 200\,\mu$s, confirming a result seen by GASP (Shearer, 2008). And there is also an optical response to the Crab's giant radio pulses, as seen by Shearer et al. (2003), Collins et al. (2012) and confirmed by Strader et al. (2013).

Table 2.6 summarises the range of technologies available and the current time resolutions that they have achieved, as well as the future directions in which they are heading. Whilst much of this has been targeted at the physics of rapidly rotating pulsars, it is worth noting that accretion processes around BH and NS compact objects also require high time resolution. The order of magnitude free-fall timescale t is $\sim(R^3/2GM)^{1/2}$, and while this is around $\sim$2 s for a WD, it is $\sim 100\,\mu$s for a NS or stellar-mass BH, so the study of such processes clearly requires HTRA. Actually, even for WDs, faster time resolution than this is required when eclipsing systems are studied, and this was shown by O'Donoghue et al. (2006) using frame-transfer CCDs to exploit the large collecting area of SALT on the polar SDSS J015543+002807 (see Figure 2.13).

2.4. HTRA Future Developments and New Technologies

Across all wavelengths, we are seeing research results that are taking the current instrumentation described in Table 2.6 from the second to millisecond regime down towards nanosecond resolutions, as well as improving on their levels of QE (aiming to reach >70 per cent). The capabilities of instruments such as OPTIMA on the next decade's European Extremely Large Telescope (e-ELT) are shown in Table 2.7, finally

https://doi.org/10.1017/9781316831984.003 Published online by Cambridge University Press

TABLE 2.6. HTRA Technologies and Capabilities*

Detector	Time Resolution	QE	R ($E/\Delta E$)	Array Size (pixels)	Instrument
CCD (standard)	secs	90 %	-	$>10^7$	(common)†
CCD (FT‡)	5 ms	90 %	-	$>10^6$	ULTRACAM†
EMCCD	1 ms	90 %	-	$>10^6$	ULTRASPEC†, GASP
pnCCD	0.01 ms	90 %	-	$>10^6$	XMM-EPIC, AO systems
APD, SPAD	ns	80 %	-	∼5	OPTIMA
	ns	60 %	-	1	GASP
	0.1 ns	60 %	-	4	Iqueye
STJ	ns	>90 %	5	<100	S-Cam
TES	ns	>90 %	>20	<100	ATHENA
MKIDs	ns	>90 %	>50	$>10^4$	ARCONS

* From Shearer et al. (2010) and Kanbach & Spruit (2008) at `www.astro-opticon.org/agendas_minutes/porto_presentations/Kanbach.pdf`.
† See Chapter 3 by V. Dhillon in this volume.
‡ Frame transfer.

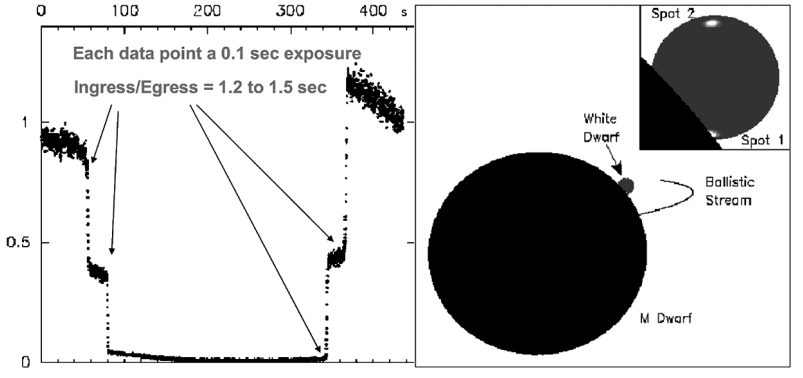

FIGURE 2.13. (Left) SALTICAM fast CCD-photometry of SDSS J015543+002807 on 2005 Sep 6, focussing on the ∼6 min eclipse of the magnetic WD. The 0.1 s time resolution afforded by frame-transfer CCDs meant that not only were the eclipses of each of the two magnetic poles clearly revealed, but their physical extent was also resolved. (Right) Schematic showing how the (very) faint M dwarf companion of SDSS J015543+002807 occults first one magnetic pole (Spot 1) on the WD, and then the other. Based on results published in O'Donoghue et al. (2006).

being able to study the other much fainter pulsars that have not yet been possible. The ultimate goal here is to achieve picosecond time resolution with ∼GHz count rate capabilities, so as to approach the limits of 'quantum optics' (Barbieri et al., 2012). Indeed, their prototype instruments, using SPADs (single-photon APDs) in continuous Geiger mode, have already reached 35 ps time resolution at count rates of <15 MHz – these are the *Aqueye* and *Iqueye* detectors that have been used on the Asiago 1.8 m telescope and the New Technology Telescope (NTT), respectively (Barbieri et al., 2012), which gave the Crab Pulsar light curves shown in Figure 2.14. A foretaste of what should be achievable with e-ELT, in a single rotation of the Crab Pulsar at 30 micro-s bcs resolution, is also shown in Figure 2.14.

https://doi.org/10.1017/9781316831984.003 Published online by Cambridge University Press

TABLE 2.7. Optical Pulsar Properties*

Pulsar	Spin Period (ms)	m_B	Photons per rotation VLT	ELT
Crab	33	16.8	3,300	63,000
PSR0540-69	50	23	13	300
Vela	89	24	10	200
PSR0656+14	385	25.5	11	230
Geminga	237	26	4	90
Crab in M31	33	29.6	1	15
Sky b/g 0.3" aperture		*21/sq arcsec*	120	2,400

*Update of Shearer (2008) and Shearer et al. (2010).

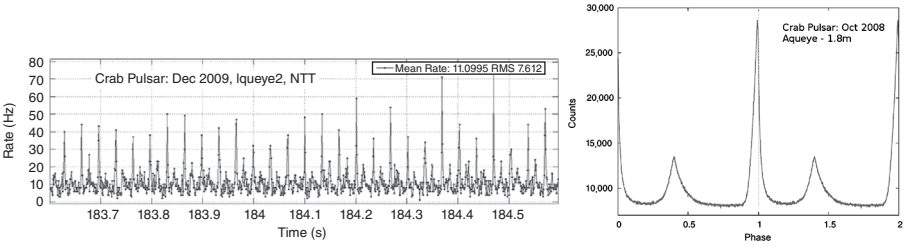

FIGURE 2.14. (Left) Individual pulses from the Crab observed in Dec 2009 using the SPADs of Iqueye2 (Barbieri et al., 2012). (Right) A half-hour folded light curve of the Crab obtained in Oct 2008 with Aqueye on the Asiago 1.8 m telescope (Germanà et al., 2012). Simulations show that it will be possible to obtain comparable quality light curves in a *single* rotation of the Crab Pulsar using the ELT, and will contain a total of 63,000 photons!

2.4.1 *Next-Generation X-ray HTRA*

The extraordinary longevity (~ 50 yrs) of LAPCs as the workhorses for HTRA work in X-ray astronomy has come about through the lack of any viable replacement for this simple technology, whose enormous strength is that they can be constructed with large collecting areas. That may be about to change, and it has come about through a spin-off from A Large Ion Collider Experiment (ALICE), one of the LHC experiments at European Organization for Nuclear Research (CERN). ALICE has an inner tracking system that incorporates a large area ($\sim 1.5\,m^2$) of silicon drift detectors, or SDDs. Their mode of operation (shown schematically in Figure 2.15) has the charge deposited in the Si by an incident photon drifting to the collection anodes as a result of the 360V/cm drift field. The drift is fast ($<5\,\mu$s), the energy range is wide (2–50 keV, and with good resolution, ~ 250 eV) and large collecting areas can be constructed with a mass per unit area one-third that of LAPCs. Mechanical collimation of the field of view, provided by glass honeycombs based on the MCP concept, is required. The most ambitious proposals to exploit SDDs have been the Large Observatory for X-ray Timing (LOFT, which at $\sim 10\,m^2$ would be ten times the collecting area of *RXTE*, see Zane and LOFT Detector's Group, 2014) and the slightly smaller (just three times the size of *RXTE*) Advanced X-ray Timing Array (AXTAR, see Chakrabarty et al., 2008). As yet, neither of these proposed missions have been accepted, but one that has is the Neutron star Interior Composition ExploreR (NICER), which launched in 2017. Located on the International Space Station (ISS), NICER uses 56 non-imaging foil concentrators (6′ field of view) with

https://doi.org/10.1017/9781316831984.003 Published online by Cambridge University Press

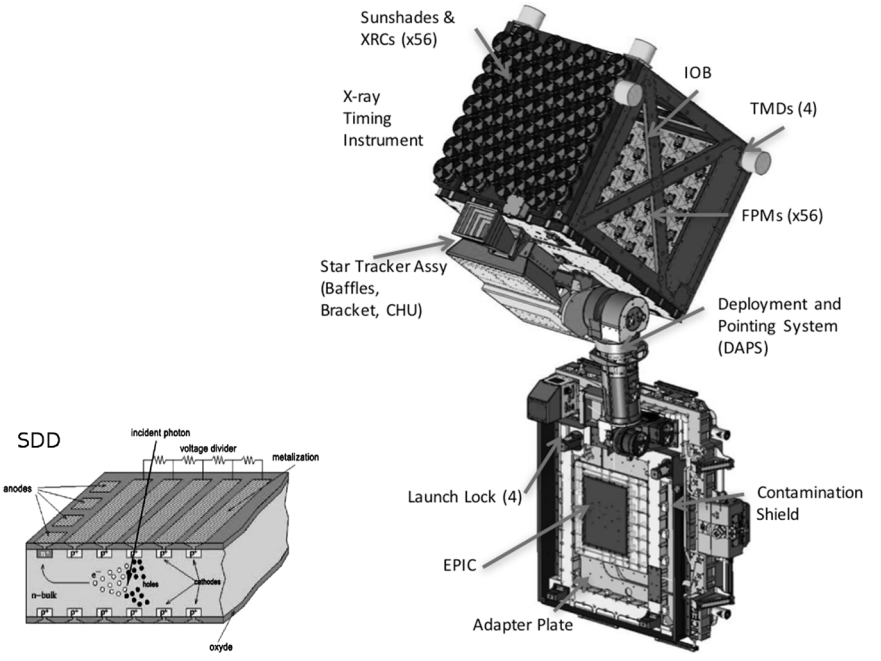

FIGURE 2.15. Schematic (left, from Zane and LOFT Detector's Group, 2014) of a silicon drift detector (SDD), the solid-state equivalent of LAPCs. Derived from LHC technology developments, they form the detection system for the NICER mission (right, from Arzoumanian et al., 2014), which launched in 2017. It achieves its large collecting area using 56 replicated foil concentrators and is mounted on the ISS. © 2014 Society of Photo Optical Instrumentation Engineers.

about double the collecting area of *XMM-Newton* to bring X-rays onto its suite of SDD detectors, sensitive from 0.2 to 12 keV and with time resolution of 0.1 μs (see Gendreau et al., 2012). Optimised for X-ray pulsars and accreting neutron stars, NICER aims to obtain the most precise constraints yet on the NS equation-of-state through its NS mass and radius measurements.

What about *Chandra* and *XMM-Newton*, the replacements for the main X-ray observatories of the last 15 years? Although providing superb imaging and hence unparalleled studies of the faint X-ray sky, they are very restricted in terms of HTRA, as described in Section 2.3. Replacing and enhancing these observatories is the task of the Advanced Telescope for High ENergy Astronomy, ATHENA, currently in a Phase A study by ESA with a target launch date of 2028 (Nandra et al., 2013). While high-efficiency X-ray spectroscopy (through the microcalorimeter concept introduced in Section 2.3.1) is a key priority of ATHENA, the ability to observe bright sources (Crab level) with $\sim 10\,\mu$s timing accuracy is also specified. Current concepts under investigation include both transition-edge sensors (TES) and Si depleted p-channel field effect transistors (DEPFETs), whose operation is shown schematically in Figure 2.16 (see Barret et al., 2015 and Barret et al., 2016). The TES is maintained close to its critical temperature at which it transitions out of its superconducting state, and hence the absorption of an X-ray photon increases the resistance by an amount related to the photon energy. This is measured by the detector electronics. An array of these will provide ~ 5 arcsec resolution and ~ 2.5 eV spectral resolution, together with 10 μs timing and ability to handle bright sources. The DEPFETs

https://doi.org/10.1017/9781316831984.003 Published online by Cambridge University Press

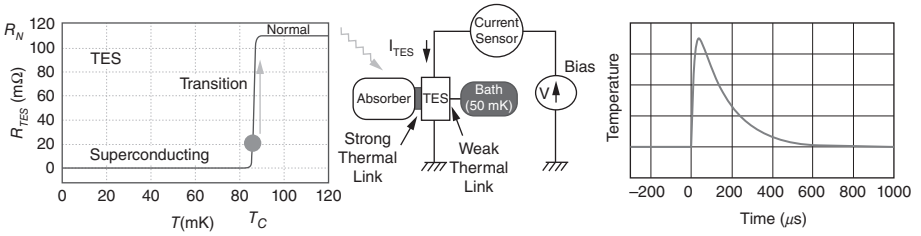

FIGURE 2.16. Operating principle of a TES, which acts as a micro-calorimeter in that the superconductor is maintained at a temperature very close to its transition point (left) from superconducting to normal conducting, and thus the energy deposited by an X-ray photon (middle) forces the material through this transition. This changes the resistance, which is detected as a change in current flow (right) (Barret et al., 2015).

offer a large matrix array of typical Si energy resolution, where incident X-ray photons produce electrons that are collected at the internal gate. As with the SDDs, bright source capability and 10 μs timing are expected.

2.4.2 *Optical/Near-Infrared Technologies*

In fact, Table 2.6 is an update of the version contained in the Shearer et al. (2010) white paper on 'HTRA in the ELT era' and is an excellent indicator of the technology development that is underway. As mentioned in that paper, there are already small arrays of devices now appearing using STJs, TESs and MKIDs (microwave kinetic inductance detectors), all of which are capable of being used over a wide range of wavelengths and are microcalorimeters. These bring the advantage of combining photon energy measurement with very high time resolution when compared to traditional CCD-based technologies. although as they exploit the properties of superconductors, they do require very low operational temperatures. However, CCDs still excel in one area – their huge array size, a property we have come to take for granted on large telescopes both on the ground and in space, where they have been (and remain) dominant in the UV-to-near-IR spectral range. It is here that these new technologies (although common for some time at FIR and sub-mm wavelengths) have been extremely limited in other spectral ranges in that they require individual pixel amplification and read-out, which greatly restricts their expandability to useful array sizes. Although the MKIDs do have potential for multiplexing to much larger array sizes, there are still considerable instrumental challenges that have to be overcome. This is described in detail by Mazin et al. (2013) and O'Brien et al. (2014), which I summarise in the following paragraphs.

The Si-based detectors that are dominant in the optical/UV region, are limited to these wavelengths by the $\sim$1eV band gap of Si, combined with the thermal noise associated with operating at temperatures above 100 K and the absence of any energy sensitivity. With the move to superconductors, this band gap is reduced by a factor of more than one thousand. The operating principle of an MKID is displayed in Figure 2.17, which is taken from Day et al. (2003). A superconducting film is the inductor (with non-zero impedance) in a resonant circuit, and the absorption of a photon breaks a large number of Cooper pairs, which changes the surface inductance, thereby changing the amplitude and phase of the resonance in the microwave read-out probe. The level of these changes is directly linked to the energy deposited by the photon, and each detector pixel can be set during manufacture to a different frequency, thereby allowing large numbers of pixels to be multiplexed, unlike with STJs. Furthermore, the very small band gap means that MKIDs can operate to 5 μ in the IR, and the detection process is extremely fast ($\sim$10 μs),

https://doi.org/10.1017/9781316831984.003 Published online by Cambridge University Press

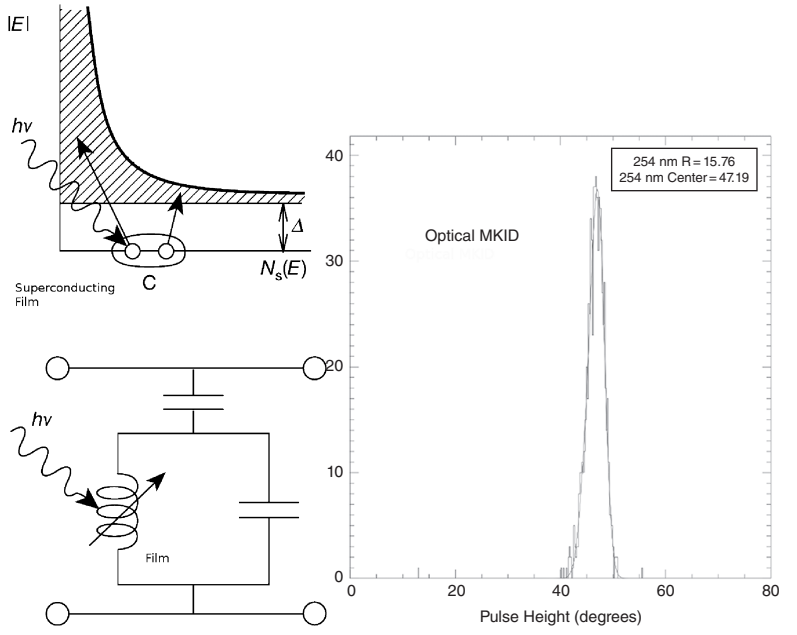

FIGURE 2.17. Operating principle of MKIDS shows a superconducting film (left, upper) absorbing a photon, breaking many Cooper pairs and thereby changing the film's surface inductance, which is sensed (lower) through a microwave resonant circuit. From Day et al. (2003). Actual R ($\sim$16) achieved in laboratory measurements of 254 nm line (right) (Mazin et al., 2013).

making them excellent for HTRA work. Their energy-sensing capability (resolving power, $R = 0.32(h\nu/F\Delta)^{1/2}$, where F is the Fano factor, and Δ the band gap) is shown in the figure with measurements of a 254 nm UV line with their TiN film.

A 1024-pixel array (of which $\sim$70 per cent is active, limited by resonator frequencies being too close together), called ARCONS (Array Camera for Optical and Near-IR Spectrophotometry), using TiN film pixels (giving R$\sim$ 10–20 at 400 nm that has been developed for optical astronomy (Mazin et al., 2013). With its use of an adiabatic demagnetisation refrigerator to deliver the 100 mK operating temperature, ARCONS is a relatively compact instrument (see Figure 2.18). Test images of Arp147 derived directly by ARCONS and can be compared (favourably) with that from HST. But the HTRA capability of ARCONS is very well demonstrated by the work on the Crab optical pulse timing relative to the giant radio pulses (Strader et al., 2013).

Future plans for MKIDs that are relevant for HTRA include Kinetic Inductance Detector Spectrograph (KIDspec) (O'Brien et al., 2014), which uses its intrinsic spectral resolving power to replace the cross-disperser in a dual-arm optical/IR echelle spectrograph. This provides $R \geq$3000 in full-range (0.35–2.4 μ) spectra of accreting compact objects and at time resolutions of <0.1s, an extremely powerful combination to sample the different kinematic components.

2.5. Final Thoughts

Both the US and European astronomy communities have put extreme environment astrophysics as one of their key research areas for the ground- and space-based telescopes under construction or being planned for the next two decades. HTRA is critical for the

https://doi.org/10.1017/9781316831984.003 Published online by Cambridge University Press

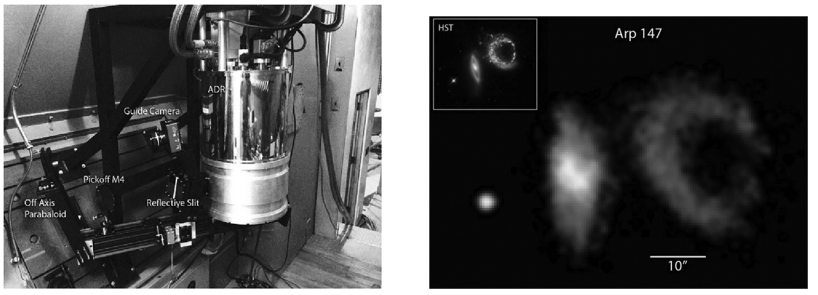

FIGURE 2.18. ARCONS, the first astronomical camera based on MKIDS detectors, shown here (left) in use at the Palomar 200-inch Hale Telescope. The use of an ADR for cooling makes it a very compact unit. An image of Arp147 (right) obtained with ARCONS at Palomar uses the spectral output of each pixel (Mazin et al., 2013).

success of these investigations. Ultimately, HTRA requires the largest telescopes for the fastest time resolutions, and the advent of e-ELT and TMT will take such work to a new level. But that will demand the use of very fast (μs), highly efficient, large-array, photon-counting detectors with intrinsic (i.e., microcalorimeter) energy resolution across a wide spectral range. Once thought to be the impossible, 'ideal' astronomical detector, there have been genuine advances towards such a device, and there is a realistic chance that it will be available by the middle of the 2020s. The greatest technological challenges (e.g., the MKIDs) will be in producing the large multiplexed arrays. Combined with access to a range of large telescopes, this will usher in a truly golden age for HTRA.

REFERENCES

Arzoumanian, Z., Gendreau, K. C., Baker, C. L. et al. 2014 (July). The Neutron star Interior Composition Explorer (NICER): Mission definition. Page 914420 of: *Space Telescopes and Instrumentation 2014: Ultraviolet to Gamma Ray. Proc. SPIE*, vol. 9144.

Barbieri, C., Naletto, G., Zampieri, L. 2012 (Apr.). Aqueye and Iqueye, very-high-time-resolution photon-counting photometers. Pages 280–282 of: Griffin, E., Hanisch, R., and Seaman, R. (eds), *New Horizons in Time Domain Astronomy*. IAU Symposium, vol. 285.

Barret, D., den Herder, J.-W. and Piro, L. 2015 (Sept.). The Athena X-ray Integral Field Unit (X-IFU). Page 4 of: Ehle, M. (ed), *Exploring the Hot and Energetic Universe: The first scientific conference dedicated to the Athena X-ray observatory*.

Barret, D., Lam Trong, T., den Herder, J.-W. et al. 2016 (July). The Athena X-ray Integral Field Unit (X-IFU). Page 99052F of: *Society of Photo-Optical Instrumentation Engineers (SPIE) Conference Series. Proc. SPIE*, vol. 9905.

Bradt, H. V., Rothschild, R. E. and Swank, J. H. 1993. X-ray timing explorer mission. *A&AS*, **97**(Jan.), 355–360.

Chakrabarty, D., Ray, P. S. and Strohmayer, T. E. 2008 (Oct.). The Advanced X-ray Timing Array (AXTAR). Pages 227–230 of: Wijnands, R., Altamirano, D., Soleri, P., Degenaar, N., Rea, N., Casella, P., Patruno, A., and Linares, M. (eds), *American Institute of Physics Conference Series*. American Institute of Physics Conference Series, vol. 1068.

Collins, P., Kyne, G., Lara, D. et al. 2013. The Galway astronomical Stokes polarimeter: An all-Stokes optical polarimeter with ultra-high time resolution. *Experimental Astronomy*, **36**(Dec.), 479–503.

Collins, P. P., Shehan, B., Redfern, M. and Shearer, A. 2009. GASP – Galway Astronomical Stokes Polarimeter. *ArXiv e-prints*, May.

Collins, S., Shearer, A., Stappers, B. et al. 2012 (Apr.). Crab Pulsar: Enhanced optical emission during giant radio pulses. Pages 296–298 of: Griffin, E., Hanisch, R., and Seaman, R. (eds), *New Horizons in Time Domain Astronomy*. IAU Symposium, vol. 285.

Day, P. K., LeDuc, H. G., Mazin, B. A., Vayonakis, A. and Zmuidzinas, J. 2003. A broadband superconducting detector suitable for use in large arrays. *Nature*, **425**(Oct.), 817–821.

Dhillon, V. S., Marsh, T. R., Stevenson, M. J. et al. 2007. ULTRACAM: An ultrafast, triple-beam CCD camera for high-speed astrophysics. *Mon Not R Astron Soc*, **378**(July), 825–840.

Fordham, J. L. A., Moorhead, C. F. and Galbraith, R. F. 2000. Dynamic-range limitations of intensified CCD photon-counting detectors. *Mon Not R Astron Soc*, **312**(Feb.), 83–88.

Fordham, J. L. A., Vranesevic, N., Carramiñana, A. et al. 2002. Phase-resolved spectroscopic imaging of the Crab Pulsar. *Astrophys J*, **581**(Dec.), 485–494.

Gehrels, N. and Cannizzo, J. K. 2015. How Swift is redefining time domain astronomy. *Journal of High Energy Astrophysics*, **7**(Sept.), 2–11.

Gendreau, K. C., Arzoumanian, Z. and Okajima, T. 2012 (Sept.). The Neutron star Interior Composition ExploreR (NICER): An Explorer mission of opportunity for soft x-ray timing spectroscopy. Page 844313 of: *Space Telescopes and Instrumentation 2012: Ultraviolet to Gamma Ray. Proc. SPIE*, vol. 8443.

Germanà, C., Zampieri, L., Barbieri, C. et al. P. 2012. Aqueye optical observations of the Crab Nebula pulsar. *Astron Astrophys*, **548**(Dec.), A47.

Harrison, F. 2015 (Sept.). NuSTAR: Probing the geometry of obscuration in the high energy X-ray band. In: Gandhi, P., and Hoenig, S. F. (eds), *TORUS2015*.

Harwit, M. 2003. The growth of astrophysical understanding. *Phys Today*, **56**(11), 38–43.

Hynes, R. I., Horne, K., O'Brien, K. et al. 2006. Multiwavelength observations of EXO 0748-676. I. Reprocessing of X-ray bursts. *Astrophys J*, **648**(Sept.), 1156–1168.

Kanbach, G., Straubmeier, C., Spruit, H. C. and Belloni, T. 2001. Correlated fast X-ray and optical variability in the black-hole candidate XTE J1118+480. *Nature*, **414**(Nov.), 180–2.

Kanbach, G., Stefanescu, A., Duscha, S. et al. 2008. OPTIMA: A high time resolution optical photo-polarimeter. Page 153 of: Milone, E. F., Leahy, D. A., and Hobill, D. W. (eds), *Astrophysics and Space Science Library*. Astrophysics and Space Science Library, vol. 351.

Kennea, J. A. 2015. The Galactic transient sky with Swift. *Journal of High Energy Astrophysics*, **7**(Sept.), 105–110.

Levan, A. J. 2015. Swift discoveries of new populations of extremely long duration high energy transient. *Journal of High Energy Astrophysics*, **7**(Sept.), 44–55.

Mackay, C. 2013. High-efficiency lucky imaging. *Mon Not R Astron Soc*, **432**(June), 702–710.

Mackay, C., Weller, K. and Suess, F. 2012 (July). Photon counting EMCCDs: New opportunities for high time resolution astrophysics. Page 845302 of: *High Energy, Optical, and Infrared Detectors for Astronomy V. Proc. SPIE*, vol. 8453.

MacKay, C., Dominik, M. and Steele, I. 2016 (Aug.). GravityCam: Wide-field, high-resolution imaging and high-speed photometry instrument. Page 99083L of: *Society of Photo-Optical Instrumentation Engineers (SPIE) Conference Series. Proc. SPIE*, vol. 9908.

Mazin, B. A., Meeker, S. R., Strader, M. J. et al. 2013. ARCONS: A 2024 pixel optical through near-ir cryogenic imaging Spectrophotometer. *Publ Astron Soc Pac*, **125**(Nov.), 1348.

McPhate, J. B., Siegmund, O. H. W., Welsh, B. Y. et al. 2012. BVIT: A visible imaging, photon counting instrument on the Southern African Large Telescope for high time resolution astronomy. *Physcs Proc*, **37**, 1453–1460.

Mitsuda, K., Kelley, R. L., Boyce, K. R. et al. 2010 (July). The High-Resolution X-Ray Microcalorimeter Spectrometer System for the SXS on ASTRO-H. Page 773211 of: *Space Telescopes and Instrumentation 2010: Ultraviolet to Gamma Ray. Proc. SPIE*, vol. 7732.

Morrissey, P. 2006 (June). A GALEX instrument overview and lessons learned. Page 62660Y of: *Society of Photo-Optical Instrumentation Engineers (SPIE) Conference Series. Proc. SPIE*, vol. 6266.

Morrissey, P. and KCWI Team. 2011 (Jan.). The Keck Cosmic Web Imager: A facility instrument for low surface brightness astronomy. Page 426.03 of: *American Astronomical Society Meeting Abstracts #217*. Bulletin of the American Astronomical Society, vol. 43.

Nandra, K., Barret, D., Barcons, X. et al. 2013. The hot and energetic universe: A White paper Presenting the Science Theme Motivating the Athena+ Mission. *ArXiv e-prints*, June.

O'Brien, K., Thatte, N. and Mazin, B. 2014 (July). KIDSpec: an MKID based medium resolution integral field spectrograph. Page 91470G of: *Ground-Based and Airborne Instrumentation for Astronomy V. Proc. SPIE*, vol. 9147.

O'Donoghue, D. 1995. High speed CCD photometry. *Balt Astron*, **4**, 519–26.

O'Donoghue, D., Buckley, D. A. H., Balona, L. A. et al. 2006. First science with the Southern African Large Telescope: Peering at the accreting polar caps of the eclipsing polar SDSS J015543.40+002807.2. *Mon Not R Astron Soc*, **372**(Oct.), 151–62.

Peacock, A., Verhoeve, P., Rando, N. et al. 1996. Single optical photon detection with a superconducting tunnel junction. *Nature*, **381**(May), 135–137.

Perryman, M. A. C., Foden, C. L. and Peacock, A. 1993. Optical photon counting using superconducting tunnel junctions. *Nucl Instrum Meth A*, **325**(Feb.), 319–325.

Perryman, M. A. C., Cropper, M., Ramsay, G. et al. 2001. High-speed energy-resolved STJ photometry of the eclipsing binary UZ For. *Mon Not R Astron Soc*, **324**(July), 899–909.

Redfern, R. M. and Collins, P. P. 2008. An ultra-high-speed Stokes polarimeter for astronomy. Page 205 of: Milone, E. F., Leahy, D. A., and Hobill, D. W. (eds), *Astrophysics and Space Science Library*. Astrophysics and Space Science Library, vol. 351.

Renker, D. 2006. Geiger-mode avalanche photodiodes, history, properties and problems. *Nucl Instrum Meth A*, **567**(Nov.), 48–56.

Rothschild, R. E., Boldt, E. A., Holt, S. S. and Serlemitsos, P. J. 1974. Millisecond temporal structure in Cygnus X-1. *Astrophys J*, **189**(Apr.), L13.

Seward, F. D. and Charles, P. A. 2010. *Exploring the X-ray Universe*. Cambridge University Press.

Shearer, A. 2008. High Time Resolution Astrophysics and Pulsars. Page 1 of: Milone, E. F., Leahy, D. A., and Hobill, D. W. (eds), *Astrophysics and Space Science Library*. Astrophysics and Space Science Library, vol. 351.

Shearer, A., Stappers, B., O'Connor, P. et al. 2003. Enhanced optical emission during Crab giant radio pulses. *Science*, **301**(July), 493–495.

Shearer, A., Kanbach, G., Slowikowska, A. et al. 2010. High time resolution astrophysics in the extremely large telescope era: White paper. Page 54 of: *Proceedings of High Time Resolution Astrophysics – The Era of Extremely Large Telescopes (HTRA-IV)*.

Sheehan, B., Kyne, G., Collins, P., Redfern, M. and Shearer, A. 2010. Detectors for high-speed polarimetric observations using GASP. Page 53 of: *Proceedings of High Time Resolution Astrophysics – The Era of Extremely Large Telescopes (HTRA-IV)*.

Siegmund, O. H. W., McPhate, J., Tremsin, A. et al. 2008 (Feb.). High time resolution astronomical observations with the Berkeley Visible Image Tube. Pages 103–114 of: Phelan, D., Ryan, O., and Shearer, A. (eds), *High Time Resolution Astrophysics: The Universe at Sub-Second Timescales*. American Institute of Physics Conference Series, vol. 984.

Słowikowska, A., Kanbach, G., Kramer, M. and Stefanescu, A. 2009. Optical polarization of the Crab Pulsar: Precision measurements and comparison to the radio emission. *Mon Not R Astron Soc*, **397**(July), 103–123.

Smale, A. P., Mason, K. O., White, N. E. and Gottwald, M. 1988. X-ray observations of the 50-min dipping source XB1916-053. *Mon Not R Astron Soc*, **232**(June), 647–660.

Steeghs, D., Perryman, M. A. C., Reynolds, A. et al. 2003. High-speed energy-resolved STJ photometry of the eclipsing dwarf nova IY UMa. *Mon Not R Astron Soc*, **339**(Mar.), 810–816.

Strader, M. J., Johnson, M. D., Mazin, B. A., et al. 2013. Excess optical enhancement observed with ARCONS for early Crab giant pulses. *Astrophys J*, **779**(Dec.), L12.

Tanaka, Y. 1989 (Nov.). Black Holes in X-ray Binaries: X-Ray Properties of the Galactic Black Hole Candidates. In: Hunt, J., and Battrick, B. (eds), *Two Topics in X-Ray Astronomy, Volume 1: X-Ray Binaries. Volume 2: AGN and the X-Ray Background*. ESA Special Publication, vol. 296.

Walker, M. F. 1956. A photometric investigation of the short-period eclipsing binary, Nova DQ Herculis (1934). *Astrophys J*, **123**(Jan.), 68.

Zane, S. and LOFT Detector's Group. 2014. LOFT – Large Observatory for X-ray Timing. *J Instrum*, **9**(Dec.), C12003.